RESEARCH ARTICLE

Eps 15 Homology Domain (EHD)-1 Remodels Transverse Tubules in Skeletal Muscle

Alexis R. Demonbreun[1]*, Kaitlin E. Swanson[2], Ann E. Rossi[3], H. Kieran Deveaux[3], Judy U. Earley[1], Madison V. Allen[1], Priyanka Arya[4], Sohinee Bhattacharyya[5], Hamid Band[5], Peter Pytel[2], Elizabeth M. McNally[1]

1 Center for Genetic Medicine, Northwestern University, Chicago, IL, United States of America,
2 Department of Pathology, The University of Chicago, Chicago, IL, United States of America, 3 Department of Medicine, The University of Chicago, Chicago, IL, United States of America, 4 Department of Genetics, Cell Biology & Anatomy, University of Nebraska Medical Center, Omaha, NE, United States of America, 5 Department of Pathology & Microbiology, Eppley Institute for Research in Cancer and Allied Diseases, University of Nebraska Medical Center, Omaha, NE, United States of America

* alexis.demonbreun@northwestern.edu

Abstract

We previously showed that Eps15 homology domain-containing 1 (EHD1) interacts with ferlin proteins to regulate endocytic recycling. Myoblasts from *Ehd1*-null mice were found to have defective recycling, myoblast fusion, and consequently smaller muscles. When expressed in C2C12 cells, an ATPase dead-EHD1 was found to interfere with BIN1/amphiphysin 2. We now extended those findings by examining *Ehd1*-heterozygous mice since these mice survive to maturity in normal Mendelian numbers and provide a ready source of mature muscle. We found that heterozygosity of EHD1 was sufficient to produce ectopic and excessive T-tubules, including large intracellular aggregates that contained BIN1. The disorganized T-tubule structures in *Ehd1*-heterozygous muscle were accompanied by marked elevation of the T-tubule-associated protein DHPR and reduction of the triad linker protein junctophilin 2, reflecting defective triads. Consistent with this, *Ehd1*-heterozygous muscle had reduced force production. Introduction of ATPase dead-EHD1 into mature muscle fibers was sufficient to induce ectopic T-tubule formation, seen as large BIN1 positive structures throughout the muscle. *Ehd1*-heterozygous mice were found to have strikingly elevated serum creatine kinase and smaller myofibers, but did not display findings of muscular dystrophy. These data indicate that EHD1 regulates the maintenance of T-tubules through its interaction with BIN1 and links T-tubules defects with elevated creatine kinase and myopathy.

Introduction

Loss of function mutations in *BIN1*, the gene encoding the membrane trafficking protein BIN1/amphiphysin 2, cause severe forms of myopathy with muscle weakness evident at birth [1,2]. Autosomal dominant mutations in *DNM2*, the gene encoding dynamin 2, another membrane trafficking protein, also cause myopathy resulting in both mild and severe forms of disease [3,4]. Dynamins are large GTPases that alter actin dynamics and membrane trafficking by

forming rings encasing membrane tubules and aiding in the fission process. Although dynamin is ubiquitously expressed, *DNM2* mutations manifest with muscle weakness presumably through gain-of-function activity that targets vesicles and membrane remodeling in muscle. Recently, it has been shown that partial reduction of dynamin 2 protein was sufficient to rescue the muscle pathology of myotubularin-deficient mice, suggesting a potential therapeutic role for this large family of proteins [5]. Myotubularin is a phosphoinositide phosphatase, and loss of function *MTM1* mutations also cause myopathy [1].

Structural studies have shown a similarity between the G-domain of Eps15 Homology Domain (EHD) proteins and dynamin, predicting a "pinchase" role for EHDs in regulating membrane fission by assembling into spiral rings. This function was confirmed by studies with lamprey EHD, l-EHD, in which l-EHD strongly inhibited excessive assembly of dynamin and the formation of elongated vesicular structures [6]. Distinct from dynamin, EHDs directly associate with other proteins through the EH domain which binds with proteins containing the asparagine-proline-phenylalanine (NPF) motif typically followed by acidic residues such as aspartic acid and/or glutamic acid [7]. This specific binding sequence is found in EHD binding partners such as BIN1, Rab-interacting proteins, and the ferlin family proteins myoferlin and Fer1L5. All of these proteins are implicated in aspects of vesicle trafficking and recycling [8,9].

The EHD family of proteins regulates multiple steps of endocytic and vesicle trafficking [10,11]. The mammalian EHD family consists of four proteins, EHD1-4, while there is a single EHD protein in both *Drosophila* (PAST-1) and *C. elegans* (RME-1). The EHD proteins contain a P-loop within the N-terminal G-domain that hydrolyzes ATP, a central helical region, and a C-terminal EH domain. Mutations in the P-loop or coiled-coil region have been shown to interfere with ATP hydrolysis and alter oligomerization, a property essential for function [12]. Despite the absence of a transmembrane domain, EHD family members associate with the membrane of vesicles and tubular structures. The ability of EHDs to associate with and form membrane-bound tubules requires the P-loop, oligomerization, and protein/protein interaction domains. BIN1 coimmunoprecipitates and colocalizes with EHD1, and EHD1 functions in conjunction with BIN1 to refine the length and width of membrane tubules [9,13]. EHD family members are highly related, approximately 70% between EHD1 and EHD2 and 86% between EHD1 and EHD3, although patterns of tissue expression are distinct.

During muscle development, EHD proteins are differentially expressed. EHD2 is expressed early in myoblasts before fusion to multinucleate myotubes, while EHD1 and EHD4 are expressed during myotube formation and maturation [8]. In myotubes that have been wounded, EHD2 is recruited to the site of sarcolemmal damage [11]. In the failing heart, EHD3 levels are increased, suggesting a role for EHD3 in the remodeling cardiomyocyte [14]. Mature skeletal muscle relies on deep membrane invaginations, referred to as transverse, T-tubules, in order to uniformly trigger rapid Ca^{2+} release throughout the myofiber and orchestrate muscle contraction [15–17]. The remodeling of T-tubules in mature myofibers is not well understood, but the presence of a rich T-tubule network provides the normal intracellular localization to scaffold Ca^{2+}-handling proteins including the ryanodine receptor and other Ca^{2+} channels [16,18,19].

Because EHD1 is expressed in muscle and regulates membrane trafficking, we examined mice heterozygous for an *Ehd1* gene deletion that produces partial reduction of EHD1 [8,13,20]. *Ehd1*-heterozygous muscle was associated with elongated and ectopic T-tubule structures in skeletal muscle and reduced force production *ex vivo*. T-tubule associated Ca^{2+}-handling proteins, including the dihydropyridine receptor (DHPR) and junctophilin, were mis-expressed with increased DHPR and reduced junctophilin in *Ehd1*-heterozygous muscle. The disrupted expression of Ca^{2+}-handling proteins may explain the observed muscle weakness in *Ehd1*-heterozygous muscle. Expression of dominant-negative EHD1 in muscle was

found to induce similar T-tubule defects with aggregation and excessive accumulation, suggesting that EHD1 acts to negatively remodel the T-tubule.

Results

Transverse-tubule abnormalities in *Ehd1*-heterozygous muscle

The *Ehd1*-null allele was previously generated, and most homozygous null *EHD1* mice die *in utero* or at birth [20,21]. The surviving mice develop male infertility [13,20]. We previously examined myoblasts from *Ehd1* null mice finding evidence for delayed endocytic recycling and smaller myofibers [13]. Using a cell culture system, we found evidence for an interaction between BIN1 and EHD1, and in the few surviving mice, complete loss of EHD1 in *Ehd1*-null mice resulted in disorganized T-tubules [13].

BIN1 normally is essential for normal T-tubule development in muscle helps tether DHPR to the T-tubule [13,22–25]. To determine whether endogenous BIN1 was altered in *Ehd1*-heterozygous muscle, myofibers were isolated and stained with antibodies to BIN1 and DHPR. *Ehd1*-heterozygous fibers displayed disordered T-tubules marked by BIN1 and DHPR fluorescence (Fig 1). The DHPR puncta were highly disorganized with ectopic T-tubules (Fig 1, white arrowhead), similar to the disorganized T-tubule pattern seen in muscle from dysferlin-null mice, a model of Limb girdle muscular dystrophy 2B [22]. High magnification imaging showed BIN1 elongation that extended beyond the DHPR domain (Fig 1, yellow arrowhead), consistent with expansion of the membranous network. Wildtype T-tubules, marked by BIN1 and DHPR fluorescence, were found in the expected ordered pattern, with rare instances of elongated BIN1 fluorescence (Fig 1). Large aggregates of T-tubules were visualized in *Ehd1*-heterozygous fibers, with 27% of fibers showing this pattern (3/11 fibers). These aggregates were positive for DHPR and BIN1, and this compared to 0% of aggregates in control, wildtype muscle fibers (0/9 fibers) (Fig 1, white arrow).

Ca^{2+}-handling proteins are enriched in T-tubules, and DHPR is one of the major proteins that regulate Ca^{2+} release to coordinate muscle contraction [19,23]. Immunoblot and density analysis revealed *Ehd1*-heterozygous muscle showed an increase of both BIN1 (+2.25 fold), and DHPR (+5.4 fold) protein levels compared to WT (Fig 2A, n≥3 of each genotype). Junctophilins span the endoplasmic reticulum (ER) / sarcoplasmic reticulum (SR) membranes to stabilize T-tubules and to facilitate attachment to the plasma membrane [26]. Loss of JP1 or JP2 in mice results in disorganized triads and reduced Ca^{2+} homeostasis and ultimately embryonic lethality [26,27]. *Ehd1*-heterozygous skeletal muscle had a 13-fold decrease of JP2 protein compared to controls (Fig 2B, n≥3 of each genotype) while JP1 protein expression was unchanged between *Ehd1*-heterozygous skeletal muscle and controls (Fig 2C, n = 2 of each genotype). The increased expression of BIN1 and DHPR in addition to the reduction of JP2 in *Ehd1*-heterozygous mice correlates with disorganization of the T-tubule system. These data provide evidence of a molecular network that functions to control T-tubule organization and is dysregulated in *Ehd1*-heterozygous mice.

Ultrastructural T-tubule overgrowth in *Ehd1*-heterozygous muscle

T-tubule abnormalities are seen in multiple myopathic states, including the central nuclear myopathies and dysferlin-mediated myopathies [1,2,28–31]. EHD1 regulates the formation of small intracellular tubules in cell culture, and complete loss of *Ehd1* produced T-tubule elongation [13]. Ultrastructural analysis of *Ehd1*-heterozygous muscle displayed similarly elongated (Fig 2D, black arrow) and ectopic (Fig 2D, black dotted arrow) T-tubules, indicating that partial reduction of EHD1 is sufficient to cause this effect. In mammalian muscle sarcomeres, a triad is composed of a T-tubule centered between two terminal cisternae of sarcoplasmic
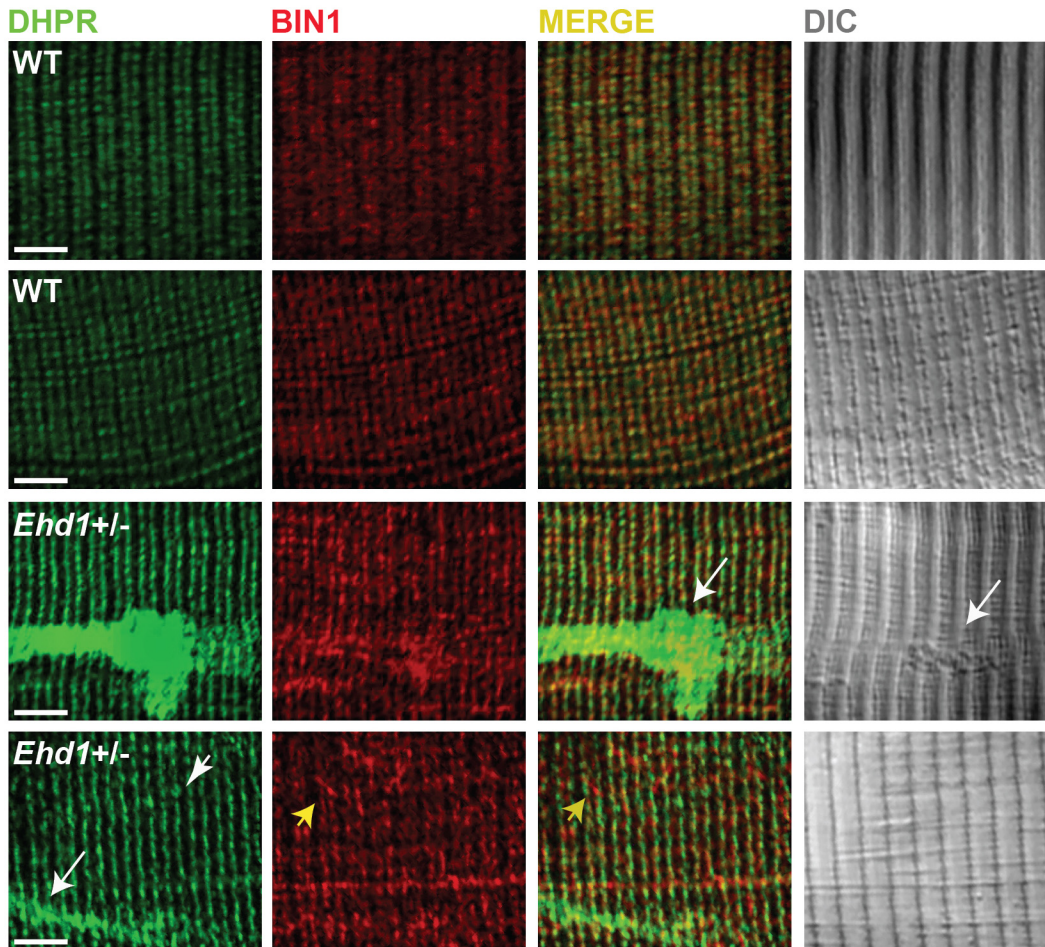
Fig 1. Disordered T-tubules in *Ehd1*-heterozygous muscle. Myofibers were immunostained with anti-BIN1 (red) and anti-DHPR (green) antibodies. Representative myofibers are shown. *Ehd1*-heterozygous (*Ehd1*+/-) fibers displayed disorganized (white arrowhead) and aggregated (white arrow) T-tubule structures in 27% of myofibers, marked by DHPR, also evidenced in DIC images compared to 0% in control fibers. *Ehd1*-heterozygous muscle with extensive BIN1 fluorescence extending beyond DHPR staining (yellow arrowhead). Scale 5µm.

doi:10.1371/journal.pone.0136679.g001

reticulum (SR). Magnified ultrastructural images of *Ehd1*-heterozygous muscle showed duplicated triad structures, containing additional T-tubule and SR units (Fig 2E). Additional images from *Ehd1*-heterozygous muscle stained with potassium ferricyanide, which colors the T-tubules black, outlined the duplicated T-tubule structures seen within a single triad (Fig 2F). T-tubule abnormalities were quantified from 2-D ultrastructural images. *Ehd1*-heterozygous muscle showed an increase in tubule structure abnormalities, 12.5%, compared to 1.7% in control muscle (Fig 2G, p = 0.04, >400 structures analyzed per genotype). This data indicates that even partial reduction of EHD1 is sufficient for T-tubule remodeling.

Reduced force production in *Ehd1*-heterozygous muscle

To assess muscle function *ex vivo*, muscle mechanical measurements were using the *extensor digitorum longus* (EDL) muscle using a force transducer. Representative force tracings from 8-week-old wildtype and *Ehd1*-heterozygous mice showed reduced specific force production in *Ehd1*-heterozygous muscles (Fig 3A). Twitch force in *Ehd1*-heterozygous EDLs (9.73 mN/mm^2) was reduced compared to wildtype (12.08 mN/mm^2) (Fig 3B, n = 5 mice each, p<0.05).
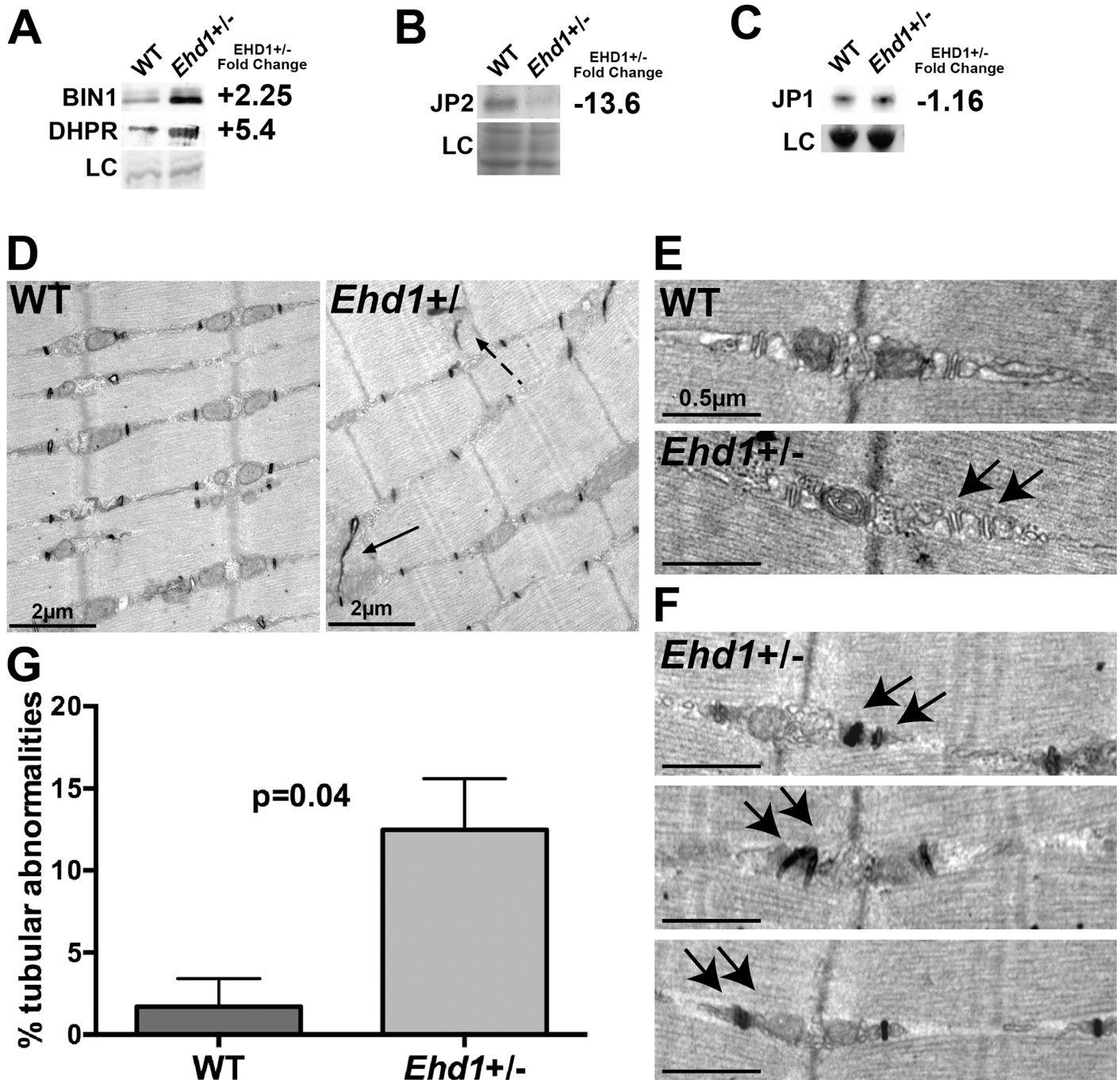
Fig 2. **Misexpression of triad proteins and expansion of the T-tubule compartment in *Ehd1*-heterozygous muscle.** (A) BIN1 and DHPR levels are increased +2.25 and +5.4 fold in *Ehd1*+/- quadriceps muscle compared to WT correlating with the increase in T-tubule structures. Gel code bands are shown as a loading control (LC). (B) Junctophilin 2 (JP2) protein levels were decreased 13-fold in *Ehd1*+/- quadriceps muscle compared to wildtype controls. Gel code stained bands are shown as a loading control (LC). (C) Junctophilin 1 (JP1) protein levels were similar in *Ehd1*+/- quadriceps muscle compared to wildtype controls. Gel code stained bands are shown as a loading control (LC). (D) Ultrastructural analysis reveals ectopic (dotted arrow) and elongated (arrow) T-tubules in 8-week-old *Ehd1*-heterozygous muscle (*Ehd1*+/-) stained with potassium ferricyanide to color the T-tubule structures black. (E) *Ehd1*-heterozygous muscle contains duplicated triads containing 2 T-tubules (black arrows) and 3 sarcoplasmic reticulum (SR) in 1 triad unit. Scale 0.5µm. (F) *Ehd1*-heterozygous muscle stained with potassium ferricyanide, outlines duplicated T-tubule structures (two black arrows). Scale 0.5µm. (G) Ultrastructural analysis of 2-D images reveals increased tubule abnormalities in *Ehd1*-heterozygous muscle, 12.5%, compared to 1.7% in control muscle (n>400 structures per genotype, p = 0.04).
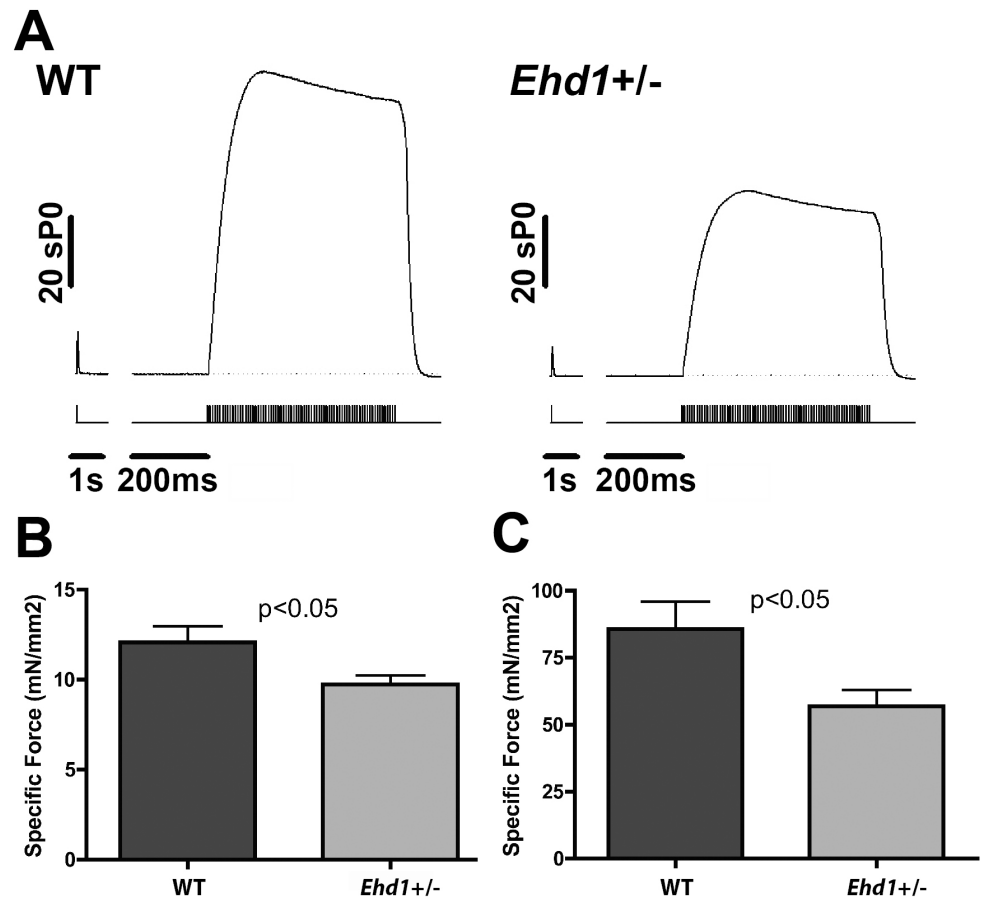
Fig 3. Reduction in EDL force production in *Ehd1*-heterozygous muscle. (A) Representative traces from 8-week male WT and *Ehd1*-heterozygous (*Ehd1*+/-) EDL muscles with stimulation pulses marked below the force traces. *Ehd1*+/- muscle has reduced force. (B) *Ehd1*+/- EDL muscle has reduced twitch force (n > 5 per genotype, p<0.05). (C) *Ehd1*+/- EDL muscle has reduced maximum tetanic force (n > 5 per genotype, p = 0.05).

doi:10.1371/journal.pone.0136679.g003

Maximal tetanic force production in *Ehd1*-heterozygous (56.92 mN/mm^2) muscle was significantly reduced compared to wildtype (85.72 mN/mm^2) (Fig 3C, n = 5 mice each, p<0.05). These data show that reduction of EHD1 is sufficient to cause appreciable muscle weakness in mice.

Ehd1-heterozygous mice have myopathy but not dystrophy

It was shown previously that the complete genetic loss of *Ehd1* ablated EHD1 protein expression in multiple tissues including heart and skeletal muscle [20,21]. Intermediate levels of EHD1 were evident by immunoblot in *Ehd1*-heterozgous cardiac muscle [20]. Skeletal muscle from 8–12 week old wildtype and *Ehd1*-heterozygous mice was assessed by immunoblot utilizing antibody against EHD1 (S1A Fig). Gelcode was used as a loading control. *Ehd1*-heterozygous skeletal muscle has a reduction in EHD1 protein level (30% compared to wildtype 88% p = 0.003, n = 4 muscles per genotype).

The pathway of muscle degeneration and regeneration is often characterized by discrete histological features including internalization of nuclei, representative of myofiber repair after injury, increased fatty and immune infiltration, and abnormal fiber distribution. In progressive

muscular dystrophy, these factors increase over time, as myofiber degeneration outpaces myofiber repair. To determine if *Ehd1*-heterozygous mice display signs of muscular dystrophy, due to the decreased levels of EHD1, we evaluated the muscle histopathology of both young and aged mice. *Ehd1*-heterozygous muscles contained multiple small myofibers versus age-matched wildtype controls, indicative of fiber splitting and/or regeneration (S1B Fig). The mean cross-sectional area (CSA) of *Ehd1*-heterozygous myofibers was reduced in muscles from young animals (S1C Fig, p = 0.003 for triceps muscles). We examined the distribution of myofiber size in muscle and found that 8-week-old *Ehd1*-heterozygous muscle specifically lacked the largest myofibers and contained an increased number of smaller myofibers (S1D Fig). To assess this distribution, we compared variances utilizing an F-test and determined that there was an unequal distribution of fibers (p<0.0001). Internal nuclei were rarely seen in *Ehd1*-heterozygous triceps muscle and WT controls at 8-weeks of age (p = 0.64, n = 3 mice per genotype, n>1000 fibers). There was no evidence of fibrosis or fatty infiltration seen in muscular dystrophy in young or old animals (S1E Fig).

Ehd1-heterozygous mice have significantly elevated serum creatine kinase

Creatine kinase (CK) generates phosphocreatine to allow more ready use of ATP in high energy demand cells like myofibers. CK leaks from muscle into the serum after intense exercise or injury, or in muscle disease [32]. Interestingly, serum CK levels were markedly elevated at birth (P0) in *Ehd1*-heterozygous mice (*Ehd1+/-* 4641 U/L vs WT controls 532 U/L, p<0.0001) (Fig 4A). Serum CK levels were persistently elevated in *Ehd1*-heterozygous mice throughout their lives with CK levels more than 40-fold higher than wildtype controls at all ages analyzed (n = 4 WT, n = 6 *Ehd1+/-*, p< 0.002) (Fig 4B). Blood urea nitrogen (BUN) and creatinine levels were normal in *Ehd1*-heterozygous mice, consistent with normal clearance through the kidney (BUN for *Ehd1*-heterozygous was 32.4 mg/dL versus 30.4 mg/dL for wildtype, n = 5 WT, n = 4 *Ehd1+/-*, p = 0.7; creatinine for *Ehd1*-heterozygous was 0.23 mg/dL compared to 0.26 mg/dL for wildtype controls, n = 3 WT, n = 2 *Ehd1+/-*, p = 0.4). These data indicate a muscle origin for serum CK elevation occurring in the absence of overt histopathological changes.

CK and other muscle proteins are hypothesized to leak into the serum with sarcolemmal disruption [33]. Sarcolemmal disruption can also be monitored by measuring uptake of vital tracers such as the small molecular mass marker Evans blue dye [34]. Eight-week-old wildtype and *Ehd1*-heterozygous mice were injected with dye and muscles were harvested for analysis. WT and *Ehd1*-heterozygous muscle displayed similar levels of dye uptake (Fig 4C). There was no significant difference in the dye uptake of any muscle group assayed (quadriceps (p = 0.92), gluteus/hamstring (p = 0.80), triceps (p = 0.66), gastrocnemius/soleus (p = 0.75), abdominal muscles (p = 0.81), and diaphragm (p = 0.98) between *Ehd1*-heterozygous muscle compared to wildtype controls (n = 6 WT, n = 7 *Ehd1+/-*) (S2 Fig). The absence of muscle breakdown in *Ehd1*-heterozygous muscle in the presence of markedly elevated serum CK links T-tubule defects with CK release.

Functional EHD1 is required for proper BIN1 localization and T-tubule formation in vivo

To determine if EHD1 modulates mature T-tubules, we conducted *in vivo* electroporation using plasmid expression of EHD1-mCherry or EHD1T72A-mCherry. The T72A substitution abrogates the ATPase activity of EHD proteins, creating a enzymatically dead EHD1 protein [12]. These plasmids were co-electroporated along with a plasmid expressing BIN-GFP into wildtype myofibers, and myofiber imaging was conducted seven days after electroporation to
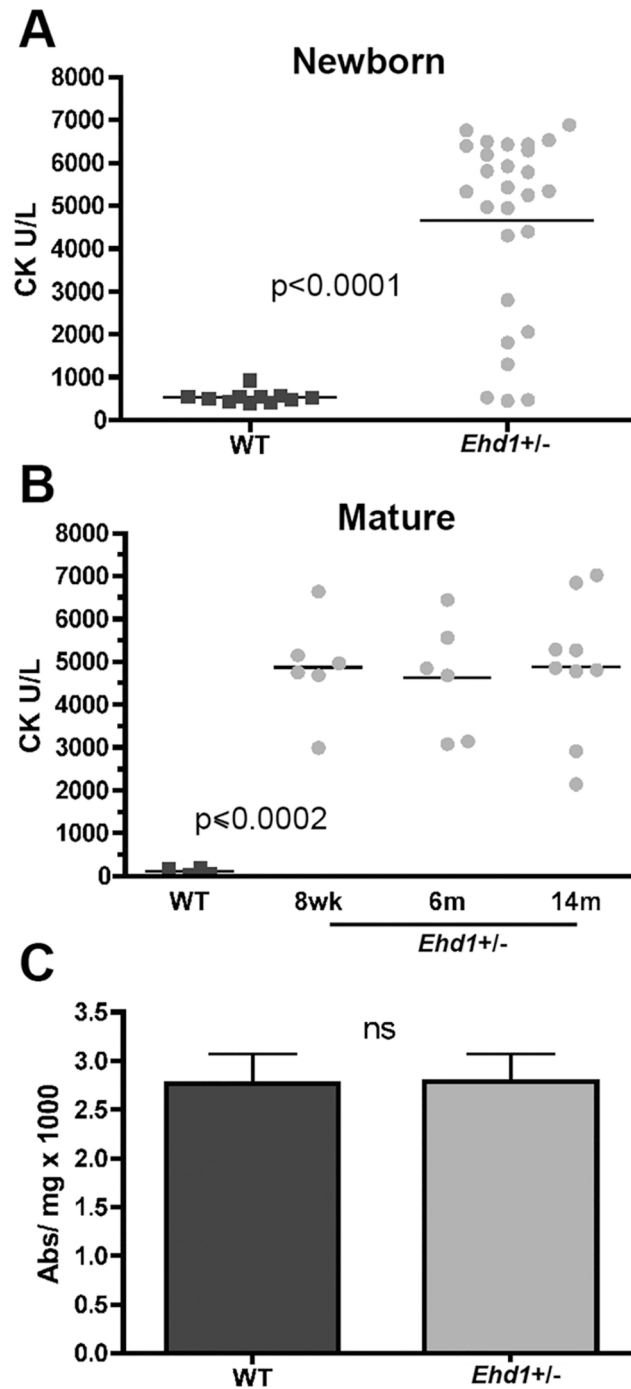
Fig 4. *Ehd1*-heterozygous mice have elevated creatine kinase levels. (A) Serum creatine kinase (CK) levels are highly elevated in *Ehd1*-heterozygous (*Ehd1*+/-) mice at birth (n > 10 of each genotype, p<0.0001). (B) CK levels are consistently elevated in *Ehd1*+/- mice at 8wk, 6m, and 14m compared to WT controls (n ≥ 6 of each genotype, p<0.0002). (C) Evans blue dye uptake was measured from excised tissues (absorbance per mg tissue). Graph expressed as an average of all tissues. Evans blue dye uptake (measured as absorbance) is similar in *Ehd1*+/- and WT (n>6 animals per genotype, ns, nonsignificant).

permit time for cell recovery and protein expression. Normally, EHD1 and BIN1 proteins localized in discrete, organized T-tubules throughout the myofiber (Fig 5A, top panel). However, when EHD1T72A was electroporated in conjunction with BIN1, EHD1T72A localized to the T-tubule less efficiently than EHD1 resulting in disrupted BIN1-mediated T-tubule formation. Specifically, expression of EHD1T72A caused ectopic and elongated BIN1-positive tubule formation in myofibers (Fig 5B, white arrow). Abnormal T-tubule formation was assessed using the directionality plugin in Fiji [35–37]. Transverse (T)- tubules are represented at an angle of 0 degrees, while any deviation of this tubule direction is expressed on the histogram accordingly. Electroporation of wildtype EHD1 and BIN1 resulted in tubules plotted only at 0 degrees, indicative of their longitudinal nature. In contrast, EHD1T72A and BIN1 expression resulted in two peaks, one peak at 0 degrees and a secondary peak at 90 degrees indicative of lateral branches developing from the longitudinal tubules in EHD1T72A expressing fibers (Fig 6). A lower magnification image of the enhanced BIN1 tubule formation caused by expression of the dominant negative EHD1T72A mutant is shown in Fig 5B (white arrow). These data suggest EHD1 negatively regulates BIN1 tubule formation *in vivo* in skeletal muscle.

Discussion

Reduced EHD1 leads to a reduction in T-tubule remodeling

The EHD1 family of proteins has been implicated in protein-protein interactions necessary for membrane trafficking and especially the formation of intracellular vesicular structures [9,13,38]. BIN1, a BAR domain containing protein implicated in membrane bending, co-immunoprecipitates and colocalizes with EHD1, and EHD1 functions in concert with BIN1 to refine the length and width of membrane tubules [9,13]. Pant et al. used *C. elegans* to discover the importance of the BIN1-EHD interaction for endocytic recycling, the process by which vesicles are returned to the membrane. The role of EHDs in trafficking and membrane tubulation was investigated in a cell-based system demonstrating a role for EHD-like proteins in vesiculation and tubulation [38]. We previously co-expressed BIN1 and EHD1 in C2C12 cells, a cell model of muscle development, finding that ectopic intracellular tubules formed in the presence of dominant negative EHD1 and that *Ehd1*-null muscle had T-tubule overgrowth [13]. Each of these cell systems lacks T-tubules, so the current findings in *Ehd1*-heterozygous muscle links partial reduction of EHD1 proteins to the maintenance and remodeling of T-tubules in mature muscle. The association of malformed T-tubules with disrupted expression of Ca^{2+}-handling proteins may account for the muscle weakness observed in *Ehd1*-heterozygous muscle. However, alternative mechanisms could lead to muscle weakness, for example the leak of CK from muscle could contribute to altered energy stores (see below).

T-tubule structure and Ca^{2+} regulation

Efficient muscle contraction requires tight control of intracellular Ca^{2+}, which is enabled by an extensive membrane network to trigger Ca^{2+} release throughout the sarcomere [16]. Skeletal and cardiac muscle cells each have deep invaginations of the surface plasma membrane, referred to as the transverse (T-) tubule network. The T-tubules are interwoven with the membranous sarcoplasmic reticulum (SR). Disruption of T-tubule structure is seen in a variety of myopathies, and collectively these disorders have been referred to as "triadopathies" [39]. Modulation of BIN1 expression has been shown to result in impaired Ca^{2+} channel trafficking and aberrant Ca^{2+} transient activity in striated muscle [24,25]. *Ehd1*-heterozygous muscle displayed excessive and disorganized T-tubules, increased BIN1 protein levels, and reduction of junctophilin 2 (JP2) protein expression. Junctophilins directly link the T-tubule and sarcoplasmic reticulum (SR) membranes, anchoring the T-tubule and maintaining the proper spacing and
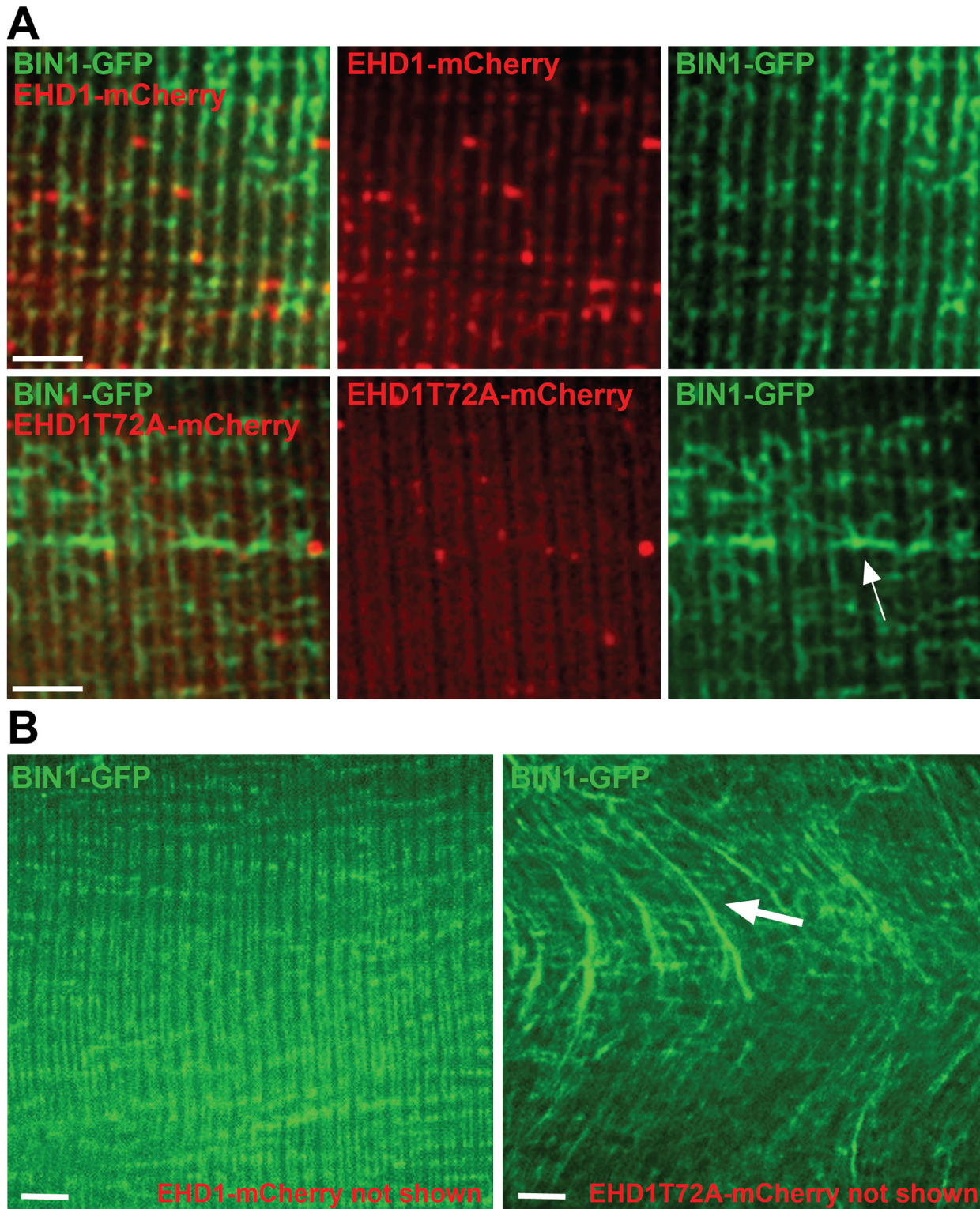
Fig 5. EHD1 modulates BIN1 mediated tubule formation *in vivo*. Myofibers were electroporated with BIN1-GFP and wildtype EHD1-mCherry or EHD1T72A-mCherry. Imaging occurred one week post-electroporation. (A & B) EHD1 and BIN1 normally align in ordered T-tubules in live skeletal muscle. Expression of EHD1T72A results in mislocalization of EHD1T72A and ectopic tubule formation (white arrow), marked with BIN1 staining. Low magnification images are shown below. Scale 5μm. BIN1 mislocalization occurred in 11/11 EHD1T72A myofibers, while 0/11 EHD1 myofibers expressed BIN1 mislocalization.

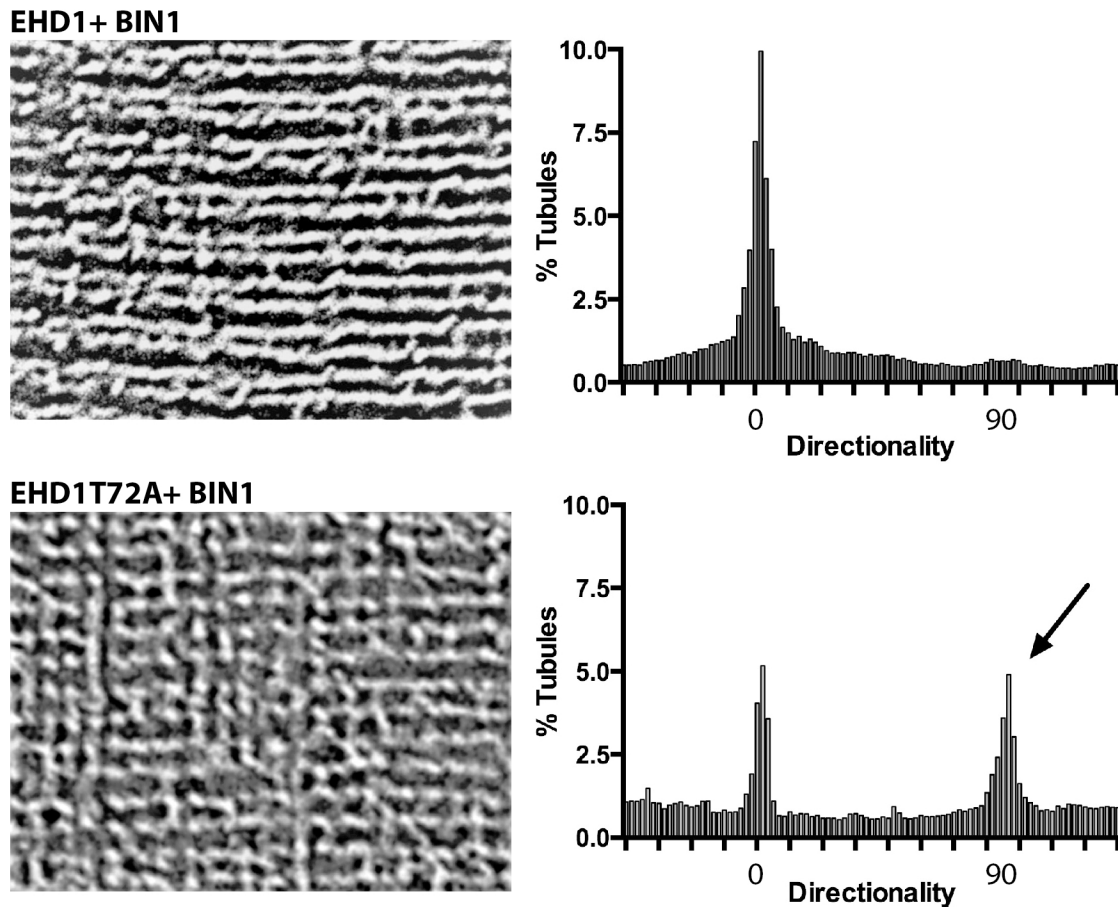**EHD1+ BIN1**

EHD1T72A+ BIN1

Fig 6. EHD1T72A is a negative regulator of BIN1 mediated tubule formation *in vivo*. Representative images of myofibers coelectroporated with BIN1-GFP and EHD1-mCherry or EHD1T72A-mCherry in wildtype myofibers. Images were processed identically in Fiji and are shown with T-tubules running horizontally. When coelectroporated with EHD1, BIN1 localizes to ordered T-tubules. Graphically this corresponds to the horizontal axis clustering around 0 degrees. Coexpression of EHD1T72A results in mislocalization of BIN1 tubules, causing lateral extensions between longitudinal tubules. Quantification shows a cluster of tubules both at 0 degrees, T-tubules, and at 90 degrees, L-tubules (arrow). Scale 5μm.

doi:10.1371/journal.pone.0136679.g006

connectivity for normal excitation-contraction (EC) coupling [26]. Genetic loss of JP1 or JP2 results in reduced Ca^{2+} signaling resulting in cardiac failure and embryonic lethality [26,27]. Reduction of JP1 or JP2 in skeletal muscle fibers results in disruption and loss of the triad structure and altered Ca^{2+} release from SR [40]. Furthermore, in cardiomyocytes, JP2 reduction resulted in altered T-tubule orientation promoting an increase in longitudinal tubule formation [41]. We hypothesize that partial loss of EHD1 results in loss of negative regulation of BIN1 activity. With unregulated BIN1 activity, T-tubules extend and grow in an uncoordinated manner, a hypothesis supported by their ectopic position within muscle. The reduction of JP2 protein expression further modulates T-tubules in excess of sarcoplasmic reticulum, and overall disorganized and inadequate triad junction formation. The abnormal morphology of T-tubules, coupled with the marked reduction of JP2, is a muscle substrate that would be expected to display abnormal Ca^{2+} handling properties. Further examination of Ca^{2+} transients, SR release, and store operated Ca^{2+} entry in *Ehd1*-heterozygous myofibers is required.

Dysferlin localizes to the T-tubule specifically at the triad junction, and loss of dysferlin (*Dysf*) results in altered Ca^{2+} homeostasis [22]. Like *Ehd1*-heterozygous mice, *Dysf*-null mice have similar T-tubule abnormalities and DHPR aggregates [22]. We have previously shown

that EHD1 weakly binds the C2B domain of DYSF and colocalizes at the T-tubule with DYSF [8,13]. The T-tubule abnormalities in *Dysf*-null mice associate with a reduction in muscle force [31,42]. Due to the co-localization of DYSF and EHD1, we hypothesize that these models share a similar set of defects. Previous studies have also shown a role for BIN1 and DYSF in stabilizing the L-type Ca^{2+} channel, which provides an additional molecular mechanism by which EHD1 deficiency may act [22,24].

Creatine kinase elevation with abnormal T-tubules

The normal function of CK within a cell is to catalyze the conversion of creatine to form phosphocreatine consuming ATP and generating ADP [43]. In addition to the elongated and ectopic T-tubule, we found markedly elevated serum CK levels in *Ehd1*-heterozygous mice without outward signs of myofiber necrosis or damage. This same finding is seen in caveolin-3-null and young ferlin-null mouse models that show mild changes in histopathology, and T-tubule abnormalities [28,31]. We hypothesize that CK may be transported from muscle into the serum by the disorganized T-tubules. Chou et al. showed human muscle biopsies from individuals with elevated serum CK levels had abnormal tubule structures compared to more than 50 healthy control subjects [44]. Chou concluded that the T-tubule was the primary location resulting in increased CK leak from muscle.

Ehd1-heterozygous muscle displays significant weakness compared to wildtype littermate muscle using *ex vivo* force experiments. Similar to *Ehd1*-null mice, *Ehd1*- heterozygous muscle contains primary, structural T-tubule deformities at an early age similar to *BIN1* and *DNM2* mutations, newly subcategorized as "triadopathies" [39]. Functional deficiencies of the T-tubule occur as a secondary consequence in a number of muscle diseases [45–47]. In contrast, there is now an emerging subset of inherited muscle disorders with primary T-tubule and membrane defects, and many of these mutations lead to congenital forms of myopathy. The data presented here indicates that EHD1 is implicated in T-tubule formation and function, and suggests that EHD1 is a potential candidate gene for unresolved genetic myopathy.

Materials and Methods

Animals

The *Ehd1*-null allele was previously generated by deleting exon 1 [20]. Mice were maintained on a mixed C57Bl/6 and 129Sv background, and housed in a specific pathogen free facility in accordance with Institutional Animal Care and Use Committee (IACUC) regulations. Euthanasia was performed through carbon dioxide or anesthetic gas inhalation followed by cervical dislocation and removal of the heart. All methods using living animals in this study were performed in ethical accordance with the American Veterinary Medical Association (AVMA) and under protocols fully approved by both the Institutional Animal Care and Use Committee (IACUC) at the University of Chicago (protocol 70619) and the IACUC at Northwestern University Feinberg School of Medicine (protocol number ISO00000911). Consistent with the approvals stipulated by these protocols, all efforts were made to minimize suffering.

Muscle analysis

Quadriceps and triceps muscles were dissected, formalin fixed and embedded in paraffin. Sections from the mid-belly of the muscle were stained with hematoxylin and eosin. Using Image J, the mean fiber cross sectional area was calculated by counting individual fibers within at least five random images from at least three *Ehd1*-heterozygous and two wildtype mice. Statistics were performed with Prism (Graphpad, La Jolla, CA) using an unpaired t-test.

Immunoblotting

Proteins in lysates of 2-3month old wildtype and *Ehd1*-heterozygous quadriceps muscles, (n ≥ 2), were transferred to membranes and were immunoblotted with anti-BIN1 (1:1000, sc-23918, Santa Cruz, Dallas, TX), rabbit polyclonal anti-EHD1 (1:5000, [10]), anti-DHPR (1:1000, ma3-920, Thermo Scientific, Rockford, IL), anti-Junctophilin 2 (1:1000, sc-51313, Santa Cruz, Dallas, TX), anti-Junctophilin 1 (1:1000, 40–5100, Thermo Scientific, Rockford, IL) antibodies. Secondary antibodies, goat anti-rabbit, and goat anti-mouse conjugated to horseradish peroxidase (Jackson ImmunoResearch) were used at a dilution of 1:2500. Blocking and antibody incubations were done in Starting Block T20 (Invitrogen, Grand Island, NY) for all antibodies and rinsed with TBS-T. Memcode and gelcode stains were used to mark proteins for loading controls (Life Technologies, Grand Island, NY). Chemiluminescence substrate, Kodak Biomax MS film, and a UVP BioSpectrum Imaging System (Upland, CA) were used for detection.

Muscle Preparation and Mechanics

Intact *extensor digitorum longus* (EDL) muscles from 8-week-old male mice were excised in regular rodent Ringer's solution (in mM: 146 NaCl, 5 KCl, 2 $CaCl_2$, 1 $MgCl_2$, and 10 HEPES, pH 7.4) essentially according to the Treat-NMD standard operating procedure. Muscles were suspended in a vertical tissue bath containing oxygenated Krebs solution (in mM: 121 NCl, 5 KCl, 1.8 $CaCl_2$, 0.5 $MgCl_2$, 0.1 EDTA, 0.4 NaH_2PO_4, 24 $NaHCO_3$, and 5 glucose, pH 7.4 with continuous bubbling 95% O_2/5% CO_2) and maintained at 25°C. The isolated muscles were stimulated with 0.5 ms pulses at 1 A via two parallel platinum electrodes flanking the muscle. The length of each EDL was adjusted to that which produced the maximal twitch force (L_0), which was measured using fine calipers. Maximal twitch and tetanic force were elicited with a series of three twitch/tetanus trains given 3 minutes apart, each train consisting of a single twitch followed by 10 secs rest then a 500-ms/150-Hz tetanus. At the conclusion of each experiment, each muscle was blotted and immediately weighed. All data were analyzed offline following data import into Clampfit software (Molecular Devices, Clampfit v10.2.0.14). The magnitude of isometric twitch and tetanus were determined as the peak twitch and peak tetanus force. All peak force measurements were normalized to cross-sectional area and expressed as specific force ($sP_{0;}$ mN/mm^2). Statistical significance was determined by t-test using Prism software.

Electron microscopy and Tubule Analysis

Quadriceps muscles from 2-month old wildtype and *Ehd1*-heterozygous mice were dissected. To visualize the T-tubules, muscles were fixed in 2.5% glutaraldehyde with 75 mM calcium chloride in 0.1mM sodium cacodylate for 3 hours, postfixed in 2% osmium tetroxide containing 0.8% potassium ferricyanide for 2 hours at 4°C, rinsed, dehydrated in ethanol, and embedded in epoxy resin modified from [29]. Samples were sectioned and stained with 1% uranyl acetate followed by lead citrate. Images were taken on a Philips CM10 electron microscope. Analysis was performed on 2D images. T-tubules were scored abnormal if ectopic duplicated or longitudinal in orientation. Three mice per genotype were analyzed equaling a total of greater than 400 structures per genotype. Statistics were performed with Prism (Graphpad, La Jolla, CA) using an unpaired t-test.

Evans Blue Dye Assay

As described previously in [48]. Briefly, Evans blue dye (E-2129, Sigma) was dissolved in phosphate buffered saline (PBS) at 10 mg/ml. Each animal received an intraperitoneal injection of

dye at 5 μl/g body weight. Approximately 48 hours after injection, tissues were harvested, finely minced, weighed and incubated at 55°C in 1ml of formamide for 2 hours with shaking. Spectrophotometric absorbance was measured at 620 nm. Statistics were performed with Prism (Graphpad, La Jolla, CA) using an unpaired t-test.

Serum Biomarker Assay

Age-matched wildtype and *Ehd1*-heterozygous blood samples were collected from the vasculature of pups sacrificed by cervical dislocation (P0) or eye bleeds (8wk, 6m, 14m) using heparin-treated capillary tubes (Fisher, Pittsburgh, PA) into serum separator tubes (Becton Dickinson, Franklin Lakes, NJ) and centrifuged for 10 min at 8000 *g*. The plasma fractions were frozen and stored at −80°C. Creatine kinase activity was determined with the EnzyChrom CK Assay kit (BioAssay Systems, Hayward, CA) and a FluoStar Optima plate reader (BMG Labtech, Cary, NC). Statistics were performed with Prism (Graphpad, La Jolla, CA) using an unpaired t-test.

Plasmids and Electroporation

EHD1-mCherry and EHD1 T72A-mCherry were described previously. pcDNA3 EHD1-GFP and EHD1 T72A-GFP were generated by subcloning a carboxy-terminal EGFP tag into EHD1 or EHD1T72A pcDNA3 using BamH1 and Xho1 restriction enzymes (New England Biolabs, Ipswich, MA). pEGFPC1-muscle Amphiphysin II (BIN1 variant 8) was purchased from Addgene (Cambridge, MA). FDB fibers were transfected by the *in vivo* electroporation methods described in detail in [49]. Muscle fibers were isolated as described and studied seven days after electroporation to allow for recovery and protein expression in the electroporated muscles. Images were acquired on the Leica SP5 II STED-CW super resolution laser scanning confocal microscope in conventional mode.

FDB preparation and Immunofluorescence Microscopy

The flexor digitorum brevis (FDB) muscle bundle was dissected and placed in 1ml of DMEM containing BSA plus collagenase solution pre-warmed to 37°C in a 12-well plate. After 2 hours, fibers were triturated in Ringers solution. Fibers were fixed on coverslips with 4% paraformaldehyde blocked in 1X phosphate-buffered saline (PBS) containing 10% fetal bovine serum and triton, and then immunostained at 1:100 with anti-DHPR (ma3-920, Thermo Scientific, Rockford, IL) and at 1:100 with anti-BIN1(sc-30099, Santa Cruz, Dallas, TX). The anti-EHD1 rabbit antibody was previously described [10]. Goat anti-rabbit conjugated to Alexa 488 and goat anti-mouse 594 were used at 1:2000. Slides were mounted with Vectashield with DAPI. Images were captured using a Leica SP5 II STED-CW super resolution laser scanning confocal microscope in standard mode.

Immunofluorescence Microscopy Tubule Analysis

Images were acquired as above and Fiji was used for the following steps. Images were rotated such that the Transverse (T)-tubules were orientated in the horizontal plane. Images were manipulated identically as follows: background fluorescence was subtracted, threshold was adjusted and then the directionality plugin was run. 0 degrees is equivalent to the transverse-tubule, while 90 degrees is equivalent to the longitudinal-tubules [35–37]. Histograms were generated in Prism (Graphpad, La Jolla, CA).

Supporting Information

S1 Fig. Decreased EHD1 expression and reduced myofiber size in *Ehd1*-heterozygous mice.
(A) Muscle lysates were prepared from 2-3m old WT and *Ehd1+/-* quadriceps muscle and
immunoblotted with anti-EHD1. *Ehd1+/-* muscle showed a 60% reduction in EHD1 protein
expression levels p = 0.003 (n = 4 per genotype). Gel code is shown as a loading control (LC).
(B) *Ehd1+/-* triceps muscle shows smaller myofibers and myofiber splitting (long arrow) at
8-weeks of age by H&E staining. (C) *Ehd1+/-* fibers have reduced mean cross sectional area
(CSA) compared to WT controls at 8-weeks (n>500 fibers, p = 0.008). (D) Histogram showing
the shift (green arrows) in myofiber CSA in *Ehd1+/-* muscle at 8-weeks (n>500 fibers,
p<0.001). (E) Hallmark signs of dystrophy were lacking in 14-month old WT and *Ehd1-
heterozygous* (*Ehd1+/-)* muscle stained with hematoxylin and eosin. Scale 50μm.
(TIF)

S2 Fig. Normal Evans Blue Dye uptake in *Ehd1*-heterzygous muscle tissues. EBD was
injected into 8-week-old WT and *Ehd1*-heterozygous (*Ehd1+/-)* mice. Forty-eight hours post
injection tissues were harvested and analyzed for EBD uptake (expressed as absorbance per mg
of tissue). The level of EBD uptake was non-significant for all muscles analyzed between WT
and *Ehd1+/-* (n ≥ 6 for both genotypes).
(TIF)

Author Contributions

Conceived and designed the experiments: ARD EMM. Performed the experiments: ARD KES
AER HKD JUE MVA PP. Analyzed the data: ARD AER PP. Contributed reagents/materials/
analysis tools: PA SB. Wrote the paper: ARD EMM PP HB.

References

1. Laporte J, Hu LJ, Kretz C, Mandel JL, Kioschis P, Coy JF, et al. (1996) A gene mutated in X-linked myo-
tubular myopathy defines a new putative tyrosine phosphatase family conserved in yeast. Nat Genet
13: 175–182. PMID: 8640223

2. Nicot AS, Toussaint A, Tosch V, Kretz C, Wallgren-Pettersson C, Iwarsson E, et al. (2007) Mutations in
amphiphysin 2 (BIN1) disrupt interaction with dynamin 2 and cause autosomal recessive centronuclear
myopathy. Nat Genet 39: 1134–1139. PMID: 17676042

3. Bitoun M, Bevilacqua JA, Prudhon B, Maugenre S, Taratuto AL, Monges S, et al. (2007) Dynamin 2
mutations cause sporadic centronuclear myopathy with neonatal onset. Ann Neurol 62: 666–670.
PMID: 17932957

4. Bitoun M, Maugenre S, Jeannet PY, Lacene E, Ferrer X, Laforet P, et al. (2005) Mutations in dynamin 2
cause dominant centronuclear myopathy. Nat Genet 37: 1207–1209. PMID: 16227997

5. Cowling BS, Chevremont T, Prokic I, Kretz C, Ferry A, Coirault C, et al. (2014) Reducing dynamin 2
expression rescues X-linked centronuclear myopathy. J Clin Invest 124: 1350–1363. doi: 10.1172/
JCI71206 PMID: 24569376

6. Jakobsson J, Ackermann F, Andersson F, Larhammar D, Low P, Brodin L (2011) Regulation of synaptic
vesicle budding and dynamin function by an EHD ATPase. J Neurosci 31: 13972–13980. doi: 10.1523/
JNEUROSCI.1289-11.2011 PMID: 21957258

7. Doherty KR, Demonbreun AR, Wallace GQ, Cave A, Posey AD, Heretis K, et al. (2008) The endocytic
recycling protein EHD2 interacts with myoferlin to regulate myoblast fusion. J Biol Chem 283:
20252–20260. doi: 10.1074/jbc.M802306200 PMID: 18502764

8. Posey AD Jr., Pytel P, Gardikiotes K, Demonbreun AR, Rainey M, George M, et al. (2011) Endocytic recycling proteins EHD1 and EHD2 interact with fer-1-like-5 (Fer1L5) and mediate myoblast fusion. J Biol Chem 286: 7379–7388. doi: 10.1074/jbc.M110.157222 PMID: 21177873

9. Pant S, Sharma M, Patel K, Caplan S, Carr CM, Grant BD (2009) AMPH-1/Amphiphysin/Bin1 functions with RME-1/Ehd1 in endocytic recycling. Nat Cell Biol 11: 1399–1410. doi: 10.1038/ncb1986 PMID: 19915558

10. George M, Ying G, Rainey MA, Solomon A, Parikh PT, Gao Q, et al. (2007) Shared as well as distinct roles of EHD proteins revealed by biochemical and functional comparisons in mammalian cells and C. elegans. BMC Cell Biol 8: 3. PMID: 17233914

11. Marg A, Schoewel V, Timmel T, Schulze A, Shah C, Daumke O, et al. (2012) Sarcolemmal repair is a slow process and includes EHD2. Traffic 13: 1286–1294. doi: 10.1111/j.1600-0854.2012.01386.x PMID: 22679923

12. Daumke O, Lundmark R, Vallis Y, Martens S, Butler PJ, McMahon HT (2007) Architectural and mechanistic insights into an EHD ATPase involved in membrane remodelling. Nature.

13. Posey AD Jr., Swanson KE, Alvarez MG, Krishnan S, Earley JU, Band H, et al. (2014) EHD1 mediates vesicle trafficking required for normal muscle growth and transverse tubule development. Dev Biol 387: 179–190. doi: 10.1016/j.ydbio.2014.01.004 PMID: 24440153

14. Gudmundsson H, Hund TJ, Wright PJ, Kline CF, Snyder JS, Qian L, et al. (2010) EH domain proteins regulate cardiac membrane protein targeting. Circ Res 107: 84–95. doi: 10.1161/CIRCRESAHA.110.216713 PMID: 20489164

15. Flucher BE (1992) Structural analysis of muscle development: transverse tubules, sarcoplasmic reticulum, and the triad. Dev Biol 154: 245–260. PMID: 1426638

16. Franzini-Armstrong C, Protasi F, Ramesh V (1998) Comparative ultrastructure of Ca2+ release units in skeletal and cardiac muscle. Ann N Y Acad Sci 853: 20–30. PMID: 10603933

17. Porter KR, Palade GE (1957) Studies on the endoplasmic reticulum. III. Its form and distribution in striated muscle cells. J Biophys Biochem Cytol 3: 269–300. PMID: 13438910

18. Block BA, Imagawa T, Campbell KP, Franzini-Armstrong C (1988) Structural evidence for direct interaction between the molecular components of the transverse tubule/sarcoplasmic reticulum junction in skeletal muscle. J Cell Biol 107: 2587–2600. PMID: 2849609

19. Jorgensen AO, Shen AC, Arnold W, Leung AT, Campbell KP (1989) Subcellular distribution of the 1,4-dihydropyridine receptor in rabbit skeletal muscle in situ: an immunofluorescence and immunocolloidal gold-labeling study. J Cell Biol 109: 135–147. PMID: 2545725

20. Rainey MA, George M, Ying G, Akakura R, Burgess DJ, Siefker E, et al. (2010) The endocytic recycling regulator EHD1 is essential for spermatogenesis and male fertility in mice. BMC Dev Biol 10: 37. doi: 10.1186/1471-213X-10-37 PMID: 20359371

21. Mate SE, Van Der Meulen JH, Arya P, Bhattacharyya S, Band H, Hoffman EP (2012) Eps homology domain endosomal transport proteins differentially localize to the neuromuscular junction. Skelet Muscle 2: 19. doi: 10.1186/2044-5040-2-19 PMID: 22974368

22. Kerr JP, Ziman AP, Mueller AL, Muriel JM, Kleinhans-Welte E, Gumerson JD, et al. (2013) Dysferlin stabilizes stress-induced Ca2+ signaling in the transverse tubule membrane. Proc Natl Acad Sci U S A 110: 20831–20836. doi: 10.1073/pnas.1307960110 PMID: 24302765

23. Lee E, Marcucci M, Daniell L, Pypaert M, Weisz OA, Ochoa GC, et al. (2002) Amphiphysin 2 (Bin1) and T-tubule biogenesis in muscle. Science 297: 1193–1196. PMID: 12183633

24. Hong TT, Smyth JW, Gao D, Chu KY, Vogan JM, Fong TS, et al. (2010) BIN1 localizes the L-type calcium channel to cardiac T-tubules. PLoS Biol 8: e1000312. doi: 10.1371/journal.pbio.1000312 PMID: 20169111

25. Tjondrokoesoemo A, Park KH, Ferrante C, Komazaki S, Lesniak S, Brotto M, et al. (2011) Disrupted membrane structure and intracellular Ca(2)(+) signaling in adult skeletal muscle with acute knockdown of Bin1. PLoS One 6: e25740. doi: 10.1371/journal.pone.0025740 PMID: 21984944

26. Takeshima H, Komazaki S, Nishi M, Iino M, Kangawa K (2000) Junctophilins: a novel family of junctional membrane complex proteins. Mol Cell 6: 11–22. PMID: 10949023

27. Ito K, Komazaki S, Sasamoto K, Yoshida M, Nishi M, Kitamura K, et al. (2001) Deficiency of triad junction and contraction in mutant skeletal muscle lacking junctophilin type 1. J Cell Biol 154: 1059–1067. PMID: 11535622

28. Galbiati F, Engelman JA, Volonte D, Zhang XL, Minetti C, Li M, et al. (2001) Caveolin-3 null mice show a loss of caveolae, changes in the microdomain distribution of the dystrophin-glycoprotein complex, and t-tubule abnormalities. J Biol Chem 276: 21425–21433. PMID: 11259414

29. Klinge L, Harris J, Sewry C, Charlton R, Anderson L, Laval S, et al. (2010) Dysferlin associates with the developing T-tubule system in rodent and human skeletal muscle. Muscle Nerve 41: 166–173. doi: 10.1002/mus.21166 PMID: 20082313

30. Liu N, Bezprozvannaya S, Shelton JM, Frisard MI, Hulver MW, McMillan RP, et al. (2011) Mice lacking microRNA 133a develop dynamin 2-dependent centronuclear myopathy. J Clin Invest 121: 3258–3268. doi: 10.1172/JCI46267 PMID: 21737882

31. Demonbreun AR, Rossi AE, Alvarez MG, Swanson KE, Deveaux HK, Earley JU, et al. (2014) Dysferlin and myoferlin regulate transverse tubule formation and glycerol sensitivity. Am J Pathol 184: 248–259. doi: 10.1016/j.ajpath.2013.09.009 PMID: 24177035

32. Brancaccio P, Lippi G, Maffulli N (2010) Biochemical markers of muscular damage. Clin Chem Lab Med 48: 757–767. doi: 10.1515/CCLM.2010.179 PMID: 20518645

33. Behringer M, Montag J, Franz A, McCourt ML, Mester J, Nosaka KK (2014) Exhaustive exercise—A near death experience for skeletal muscle cells? Med Hypotheses 83: 758–765. doi: 10.1016/j.mehy.2014.10.005 PMID: 25459151

34. Straub V, Rafael JA, Chamberlain JS, Campbell KP (1997) Animal models for muscular dystrophy show different patterns of sarcolemmal disruption. J Cell Biol 139: 375–385. PMID: 9334342

35. Jayasinghe ID, Launikonis BS (2013) Three-dimensional reconstruction and analysis of the tubular system of vertebrate skeletal muscle. J Cell Sci 126: 4048–4058. doi: 10.1242/jcs.131565 PMID: 23813954

36. Liu ZQ (1991) Scale space approach to directional analysis of images. Appl Opt 30: 1369–1373. doi: 10.1364/AO.30.001369 PMID: 20700292

37. Schindelin J, Arganda-Carreras I, Frise E, Kaynig V, Longair M, Pietzsch T, et al. (2012) Fiji: an open-source platform for biological-image analysis. Nat Methods 9: 676–682. doi: 10.1038/nmeth.2019 PMID: 22743772

38. Cai B, Giridharan SS, Zhang J, Saxena S, Bahl K, Schmidt JA, et al. (2013) Differential roles of C-terminal Eps15 homology domain proteins as vesiculators and tubulators of recycling endosomes. J Biol Chem 288: 30172–30180. doi: 10.1074/jbc.M113.488627 PMID: 24019528

39. Dowling JJ, Lawlor MW, Dirksen RT (2014) Triadopathies: an emerging class of skeletal muscle diseases. Neurotherapeutics 11: 773–785. doi: 10.1007/s13311-014-0300-3 PMID: 25168790

40. Hirata Y, Brotto M, Weisleder N, Chu Y, Lin P, Zhao X, et al. (2006) Uncoupling store-operated Ca2+ entry and altered Ca2+ release from sarcoplasmic reticulum through silencing of junctophilin genes. Biophys J 90: 4418–4427. PMID: 16565048

41. Han J, Wu H, Wang Q, Wang S (2013) Morphogenesis of T-tubules in heart cells: the role of junctophilin-2. Sci China Life Sci 56: 647–652. doi: 10.1007/s11427-013-4490-4 PMID: 23749380

42. Grose WE, Clark KR, Griffin D, Malik V, Shontz KM, Montgomery CL, et al. (2012) Homologous recombination mediates functional recovery of dysferlin deficiency following AAV5 gene transfer. PLoS One 7: e39233. doi: 10.1371/journal.pone.0039233 PMID: 22720081

43. Bessman SP, Geiger PJ (1981) Transport of energy in muscle: the phosphorylcreatine shuttle. Science 211: 448–452. PMID: 6450446

44. Chou SM, Nonaka I, Voice GF (1980) Anastomoses of transverse tubules with terminal cisternae in polymyositis. Arch Neurol 37: 257–266. PMID: 7387442

45. Andersson DC, Meli AC, Reiken S, Betzenhauser MJ, Umanskaya A, Shiomi T, et al. (2012) Leaky ryanodine receptors in beta-sarcoglycan deficient mice: a potential common defect in muscular dystrophy. Skelet Muscle 2: 9. doi: 10.1186/2044-5040-2-9 PMID: 22640601

46. Capote J, DiFranco M, Vergara JL (2010) Excitation-contraction coupling alterations in mdx and utrophin/dystrophin double knockout mice: a comparative study. Am J Physiol Cell Physiol 298: C1077–1086. doi: 10.1152/ajpcell.00428.2009 PMID: 20130206

47. Watkins SC, Hoffman EP, Slayter HS, Kunkel LM (1988) Immunoelectron microscopic localization of dystrophin in myofibres. Nature 333: 863–866. PMID: 3290684

48. Heydemann A, Huber JM, Demonbreun A, Hadhazy M, McNally EM (2005) Genetic background influences muscular dystrophy. Neuromuscul Disord 15: 601–609. PMID: 16084087

49. DiFranco M, Quinonez M, Capote J, Vergara J (2009) DNA transfection of mammalian skeletal muscles using in vivo electroporation. J Vis Exp.